BioLegend®
Find Your Balance
Research Tools for Immune Activation and Suppression
Treg, Th17, Th9, Th22, DC, NK, MDSC
08-0001-00

THE JOURNAL OF IMMUNOLOGY

STIM1-Directed Reorganization of Microtubules in Activated Mast Cells

Zuzana Hájková, Viktor Bugajev, Eduarda Dráberová, Stanislav Vinopal, Lubica Dráberová, Jirí Janácek, Petr Dráber and Pavel Dráber

This information is current as of December 22, 2010

J Immunol; Prepublished online 15 December 2010;
doi:10.4049/jimmunol.1002074
http://www.jimmunol.org/content/early/2010/12/15/jimmunol.1002074

Supplementary Data **http://www.jimmunol.org/content/suppl/2010/12/15/jimmunol.1002074.DC1.html**

Subscriptions Information about subscribing to *The Journal of Immunology* is online at http://www.jimmunol.org/subscriptions

Permissions Submit copyright permission requests at http://www.aai.org/ji/copyright.html

Email Alerts Receive free email-alerts when new articles cite this article. Sign up at http://www.jimmunol.org/etoc/subscriptions.shtml/

Advance online articles have been peer reviewed and accepted for publication but have not yet appeared in the paper journal (edited, typeset versions may be posted when available prior to final publication). Advance online articles are citable and establish publication priority; they are indexed by PubMed from initial publication. Citations to Advance online articles must include the digital object identifier (DOIs) and date of initial publication.

The Journal of Immunology is published twice each month by
The American Association of Immunologists, Inc.,
9650 Rockville Pike, Bethesda, MD 20814-3994.
Copyright ©2010 by The American Association of Immunologists, Inc. All rights reserved.
Print ISSN: 0022-1767 Online ISSN: 1550-6606.

Downloaded from www.jimmunol.org on December 22, 2010

Published December 15, 2010, doi:10.4049/jimmunol.1002074

STIM1-Directed Reorganization of Microtubules in Activated Mast Cells

Zuzana Hájková,*,[1] Viktor Bugajev,†,[1] Eduarda Dráberová,* Stanislav Vinopal,* Lubica Dráberová,† Jiří Janáček,‡ Petr Dráber,† and Pavel Dráber*

Activation of mast cells by aggregation of the high-affinity IgE receptors (FcεRI) initiates signaling events leading to the release of inflammatory and allergic mediators stored in cytoplasmic granules. A key role in this process play changes in concentrations of intracellular Ca^{2+} controlled by store-operated Ca^{2+} entry (SOCE). Although microtubules are also involved in the process leading to degranulation, the molecular mechanisms that control microtubule rearrangement during activation are largely unknown. In this study, we report that activation of bone marrow-derived mast cells (BMMCs) induced by FcεRI aggregation or treatment with pervanadate or thapsigargin results in generation of protrusions containing microtubules (microtubule protrusions). Formation of these protrusions depended on the influx of extracellular Ca^{2+}. Changes in cytosolic Ca^{2+}concentration also affected microtubule plus-end dynamics detected by microtubule plus-end tracking protein EB1. Experiments with knockdown or reexpression of STIM1, the key regulator of SOCE, confirmed the important role of STIM1 in the formation of microtubule protrusions. Although STIM1 in activated cells formed puncta associated with microtubules in protrusions, relocation of STIM1 to a close proximity of cell membrane was independent of growing microtubules. In accordance with the inhibition of Ag-induced Ca^{2+} response and decreased formation of microtubule protrusions in BMMCs with reduced STIM1, the cells also exhibited impaired chemotactic response to Ag. We propose that rearrangement of microtubules in activated mast cells depends on STIM1-induced SOCE, and that Ca^{2+} plays an important role in the formation of microtubule protrusions in BMMCs. ***The Journal of Immunology*****, 2011, 186: 000–000.**

Mast cells play a pivotal role in innate immunity, allergy, and inflammation; they express plasma membrane-associated FcεRIs, the aggregation of which by multivalent Ag–IgE complexes triggers mast cell activation resulting in the degranulation and release of inflammatory mediators such as histamine, proteases, lipid mediators, and cytokines. The first defined step in FcεRI signaling is tyrosine phosphorylation of the FcεRI β and γ subunits by Src family kinase Lyn. This step is followed by enhanced activity of Syk kinase and phosphorylation of transmembrane adaptor linker for activation of T cells. Phosphorylated linker for activation of T cells is an anchor site for phospholipase Cγ. After membrane anchoring and activation, phospholipase Cγ produces inositol 1,4,5,-triphosphate that binds to its receptors in the endoplasmic reticulum (ER). This results in Ca^{2+} efflux from the ER (1). Subsequently, depletion of Ca^{2+} from ER lumen induces Ca^{2+} influx across the plasma membrane through store-operated Ca^{2+} channels (SOCs). The influx leads to enhancement of free cytoplasmic Ca^{2+} concentration, a step that is substantial in further signaling events. The store-operated Ca^{2+} entry (SOCE) is also important for the replenishment of intracellular stores by means of sarcoendoplasmatic reticulum Ca^{2+}-ATPase (SERCA) pumps located in the ER membrane (2, 3).

The stromal interacting molecule 1 (STIM1) is a pivotal component of the SOCE pathway (4, 5). It represents the Ca^{2+} sensor responsible for communicating the depleted state of intracellular Ca^{2+} compartments to SOCs. In quiescent cells with ER filled with Ca^{2+}, STIM1 is distributed homogenously throughout the ER (6), but relocates upon release of Ca^{2+} from ER stores to distinct puncta on the ER in close proximity to the plasma membrane (5). Aggregated STIM1 activates members of the Orai family of SOCs, resulting in the opening of the plasma membrane Ca^{2+} channels and Ca^{2+} influx into the cell (7); in this way STIM1 serves as a major regulator of SOCE.

STIM1 is a microtubule-tracking protein (8, 9) and interacts with the end-binding protein 1 (EB1) that associates with the tips of growing microtubules (10, 11). Although microtubules are necessary for positioning of membrane-enclosed organelles in-

*Department of Biology of Cytoskeleton, Institute of Molecular Genetics, Academy of Sciences of the Czech Republic, 142 20 Prague, Czech Republic; †Department of Signal Transduction, Institute of Molecular Genetics, Academy of Sciences of the Czech Republic, 142 20 Prague, Czech Republic; and ‡Department of Biomathematics, Institute of Physiology, Academy of Sciences of the Czech Republic, 142 20 Prague, Czech Republic

[1]Z.H. and V.B. contributed equally to this work

Received for publication June 25, 2010. Accepted for publication November 13, 2010.

This work was supported in part by Grants 204/09/H084, 204/09/1777, 301/09/1826, and P302/10/1759 from the Grant Agency of the Czech Republic, Grants LC545, LC06063, and 1M6837805001 from the Ministry of Education, Youth and Sports of the Czech Republic, Grants KAN200520701 and M200520901 from the Grant Agency of the Czech Academy of Sciences Grant 11109 from the Grant Agency of Charles University, and by the Institutional Research Supports (AVOZ 50520514 and 50110509). S.V. was supported in part by the Department of Cell Biology, Faculty of Science, Charles University, Prague, Czech Republic.

Address correspondence and reprint requests to Dr. Pavel Dráber or Dr. Petr Dráber, Department of Biology of Cytoskeleton, Institute of Molecular Genetics, AS CR v.v.i., Vídeňská 1083, 142 20 Prague, Czech Republic (Pavel Dráber), or Department of Signal Transduction, Institute of Molecular Genetics, AS CR v.v.i., Vídeňská 1083, 142 20 Prague, Czech Republic (Petr Dráber). E-mail addresses: paveldra@img.cas.cz (Pavel Dráber) and draberpe@img.cas.cz (Petr Dráber)

The online version of this article contains supplemental material.

Abbreviations used in this article: BMMC, bone marrow-derived mast cell; BMMCL, BMMC line; BSS, buffered saline solution; $[Ca^{2+}]_i$, concentration of free intracellular calcium; EB1, end-binding protein 1; ER, endoplasmic reticulum; KD, knockdown; SCF, stem cell factor; SERCA, sarcoendoplasmatic reticulum Ca^{2+}-ATPase; shRNA, short hairpin RNA; SOC, store-operated Ca^{2+} channels; SOCE, store-operated Ca^{2+} entry; STIM1, stromal interacting molecule 1; Tg, thapsigargin; TIRF, total internal reflection fluorescence; TIRFM, total internal reflection fluorescence microscopy; YFP, yellow fluorescent protein.

Copyright © 2010 by The American Association of Immunologists, Inc. 0022-1767/10/$16.00

Downloaded from www.jimmunol.org on December 22, 2010

cluding ER (12), the role of microtubules in regulating SOCE is not fully understood. Whereas inhibition of microtubule dynamics by taxol, a microtubule stabilizer, or by knockdown (KD) of EB1 had no significant effect on SOCE (11), Ca^{2+} influx in different cell types was inhibited by microtubule depolymerizing drug nocodazole (13, 14). It has been suggested that microtubules play a facilitative role in SOCE signaling pathway by optimizing the localization of STIM1 (15).

Microtubules are involved in mast cell degranulation, because the movement of secretory granules depends on intact microtubules (16, 17). This finding is supported by demonstrations that agents inhibiting tubulin polymerization also suppress degranulation (18–20). Importantly, FcεRI aggregation triggers reorganization of microtubules and their concentration in cell periphery (17, 21). It has also been reported that translocation of granules along microtubules to plasma membranes occurred independently of Ca^{2+}, whereas the release of mediators and granule-plasma membrane fusion were dependent on Ca^{2+} (17). Although these data confirm that a microtubule network is required for mast cell degranulation, our understanding of the mechanisms responsible for microtubule formation in bone marrow-derived mast cells (BMMCs) during activation events is still limited.

In this study, we investigated the interplay between Ca^{2+} signaling and changes in microtubule distribution in the course of BMMC activation. Our results indicate that microtubules in activated cells are in protrusions that depend on STIM1 activity and Ca^{2+} influx. Whereas microtubules are not necessary for the relocation of STIM1 to puncta in close proximity to the plasma membrane in activated cells, changes in the concentration of cytoplasmic Ca^2 affect microtubule plus-end dynamics and result in dramatic modifications in cell physiology documented by chemotactic response. The results support the concept of a tight crosstalk between microtubular network and Ca^{2+} signaling machinery in the course of mast cell activation.

Materials and Methods

Reagents

Fibronectin, nocodazole, thapsigargin, probenecid, DNP-albumin, and DNP-lysine were acquired from Sigma-Aldrich (St. Louis, MO). Src-family selective tyrosine kinase inhibitor PP2 and the negative control, PP3, were obtained from Calbiochem (Darmstadt, Germany). Fluo 3-AM, Fura Red-AM, 4-methylumbelliferyl β-D-glucuronide, and Lipofectamine 2000 were purchased from Invitrogen (Carlsbad, CA), and puromycin was acquired from InvivoGen (San Diego, CA). IL-3 and stem cell factor (SCF) were from PeproTech (Rocky Hill, NJ). Restriction enzymes were bought from New England Biolabs (Ipswich, MA). SuperSignal WestPico Chemiluminescent reagents were bought from Pierce (Rockford, IL).

Abs

Mouse mAb PY-20 (IgG_{2b}) labeled with HRP and anti-STIM1(GOK) mAb (IgG_{2a}) were acquired from BD Biosciences (San Jose, CA). Rabbit Ab to α-tubulin was acquired from GeneTex (Irvine, CA). Rabbit Ab to actin, mAb TUB 2.1 (IgG_1) to β-tubulin labeled with indocarbocyanate (Cy3) and mAb SPE-7 (IgE) specific for DNP were acquired from Sigma-Aldrich. Anti-mouse and anti-rabbit Abs conjugated with HRP were purchased from Promega Biotec (Madison, WI), Alexa Fluor 488-conjugated anti-rabbit IgG Ab was acquired from Invitrogen (Carlsbad, CA), and FITC-conjugated anti-mouse IgG cross-reacting with mouse IgE were acquired from Jackson ImmunoResearch Laboratories (West Grove, PA).

To prepare mouse mAb specific for STIM1, 29-aa oligopeptide DNGSIGEETDSSPGRKKFPLKIFKKPLKK corresponding to the mouse STIM1 sequence 657-685 from the C-terminal end of the molecule (22) was synthesized by Clonestar Peptide Service (Brno, Czech Republic). A cysteine had been added to the N terminus of the peptide to allow oriented covalent coupling to the carrier proteins, maleimide-activated keyhole limpet hemocyanin, or BSA (Imject Activated Immunogen Conjugation Kit, Pierce, Rockford, IL), according to the manufacturer's directions. BALB/c mice were immunized with the peptide-keyhole limpet hemocyanin conjugate, and sera were monitored for Ab activity by ELISA on peptide-BSA conjugate as described (23). Fusion of splenocytes with mouse myeloma cells Sp2/0, screening by ELISA, cloning and production of ascitic fluids in BALB/c mice have been described previously (24). The subclasses of mAbs were identified by ISO1 isotyping kit (Sigma-Aldrich). The selected hybridoma cell line ST-01 produced Ab of the IgG_1 class.

Cell cultures and transfection

Bone marrow cells were isolated from the femurs and tibias of 6–8-wk-old BALB/c mice. All mice were maintained and used in accordance with the Institute of Molecular Genetics guidelines. The cells were differentiated in suspension cultures in freshly prepared culture medium (IMDM supplemented with antibiotics [100 U/ml penicillin, 100 μg/ml streptomycin] 10% FCS, 35 μM 2-ME, IL-3 [36 ng/ml] and SCF [36 ng/ml]). Cells were grown at 37°C in 10% CO_2 in air and passaged every 2–3 d. After 6–8 wk, ~99% of cells were identified as mast cells, expressing FcεRI and c-Kit as detected by flow cytometry. BMMCs isolated from at least three mice were used for each experiment.

Mouse BMMC line (BMMCL) was by M. Hibbs (Ludwig Institute for Cancer Research, Melbourne, Australia). In this study, the cells are denoted as BMMCL and were cultured in freshly prepared culture medium (RPMI 1640 supplemented with 20 mM HEPES, pH 7.5, 100 U/ml penicillin, 100 μg/ml streptomycin, 100 μM MEM nonessential amino acids, 1 mM sodium pyruvate, 10% FCS, and 10% WEHI-3 cell supernatant as a source of IL-3). Cells were grown at 37°C in 5% CO_2 in air and passaged every 2 d.

HEK 293FT packaging cells (Invitrogen) were grown at 37°C in 5% CO_2 in DMEM supplemented with 10% FCS and antibiotics. The cells used for lentivirus production were at passage 4–15.

BMMCL cells were transfected with DNA constructs by nucleofection using Mouse Macrophage Kit and program Y-001 on Amaxa Nucleofector II (Lonza Cologne AG, Cologne, Germany) according to the manufacturer's instructions. After nucleofection, cells were transferred into culture media supplemented with IL-3 and cultured for 24–48 h before analysis.

DNA constructs

Full-length human STIM1 cloned into pDS_XB-YFP vector (pYFP-hSTIM1) was provided by Dr. T. Meyer (5). The signal-peptide region (22), sequence 1–23 aa, of STIM1 was recloned from this vector into pmCherry_N1 from Clontech Laboratories (Mountain View, CA) upstream of mCherry, using *Eco*RI and AgeI restriction sites. The remaining part of STIM1 was recloned downstream of mCherry into the BsrGI site. The construct was verified by DNA sequencing. Expression plasmid coding mouse EB1 fused with GFP (pEB1-GFP) was obtained from Dr. Y. Mimori-Kiyosue (25). Expression plasmid coding human EB3 fused with mRFP1 (26) was obtained from Dr. A. Akhmanova (11).

Lentivirus short hairpin RNAs and virus transduction

A set of five murine STIM1 (GenBank accession number: NM_ 009287) short hairpin RNA (shRNA) constructs cloned into the pLKO.1 vector (TRCN0000175139, TRCN0000175008, TRCN0000193877, TRCN0000-193400, and TRCN0000173765) were purchased from Open Biosystems (Huntsville, AL). Aliquots of 1.4 ml Opti-MEM medium (Invitrogen) were mixed with 21 μl ViraPower Lentiviral Packaging Mix (Invitrogen), 14 μg STIM1 shRNA constructs, and 82 μl Lipofectamine 2000. The mixture was incubated for 20 min at room temperature before it was added to semiconfluent HEK-293FT packaging cells in a 150-cm^2 tissue-culture flask. After 3 d, viruses in culture supernatants were concentrated by centrifugation at 25,000 rpm for 2 h using a JA-25.50 rotor (Beckman Coulter, Palo Alto, CA). The pellets were resuspended in 1 ml of culture medium and added to 29 ml of medium, supplemented with 5 μg/ml puromycin containing 5×10^7 BMMCs or BMMCL cells. Stable selection was achieved by culturing cells for 1 wk in the presence of puromycin. Cells were pooled and analyzed for STIM1 expression by immunoblotting. Cells with the highest reduction of STIM1 protein, obtained with TRCN0000175008 (KD1) and TRCN0000193400 (KD2), were selected for additional experiments. Cells transfected with empty pLKO.1 vector were used as negative controls.

Cell activation

Cells at a concentration of 6×10^6 cells/ml were sensitized for 2 h at 37°C in IL-3– and SCF-free culture medium supplemented with DNP-specific IgE mAb (SPE-7; 1 μg/ml). The cells were then washed in buffered saline solution (BSS; 20 mM HEPES, pH 7.4, 135 mM NaCl, 5 mM KCl, 1.8 mM $CaCl_2$, 5.6 mM glucose, 2 mM $MgCl_2$), supplemented with 0.1% BSA (BSS-BSA), and challenged with various concentrations of Ag (DNP-albumin; 30–40 mol of DNP per mole of albumin) or thapsigargin.

For immunofluorescence experiments, cells at a concentration of 6×10^6 cells/ml were sensitized in suspension for 1 h at 37°C with DNP-specific

Downloaded from www.jimmunol.org on December 22, 2010

IgE (1 μg/ml) and diluted to a concentration of 1.5×10^6 cells/ml. The suspension (1 ml) was then overlaid on fibronectin-coated coverslips (immersed for 1 h at 37°C in 50 μg/ml fibronectin in 50 mM $NaHCO_3$ and rinsed in PBS) placed in a 3.5-cm tissue culture dish. Cells were allowed to attach for 1 h at 37°C, washed in BSS-BSA, and challenged for 3–5 min with Ag (DNP-albumin) at a final concentration of 100 ng/ml. To determine the time course of activation, cells were challenged with Ag for 1–10 min. For dose response curve construction, the concentration of Ag ranged from 10 to 1000 ng/ml.

Alternatively, cells were activated by pervanadate or thapsigargin, in which case the sensitization step was omitted. Pervanadate solution was prepared fresh by mixing sodium orthovanadate solution with hydrogen peroxide to get a final concentration (10 mM) of both components. The pervanadate solution was incubated for 15 min at room temperature and then diluted 1:100 in BSS-BSA. Attached cells were incubated with pervanadate solution for 15 min at 37°C. Cells were also incubated for 20 min with BSS-BSA containing 2 μM thapsigargin. To determine the time course of activation, cells were activated with thapsigargin for 5–20 min. Dose response measurements were done at thapsigargin concentrations ranging from 0.01 to 2 μM. In some experiments, $[Ca^{2+}]$-free BSS was used. Trypan blue exclusion test was used to evaluate the effect of pervanadate and thapsigargin on viability of cells.

To depolymerize microtubules, cells were treated for 1 h at 37°C with 10 μM nocodazole and activated with pervanadate or thapsigargin in the presence of nocodazole. To inhibit the activity of Src family kinases, IgE-sensitized cells were pretreated for 60 min with Src family selective tyrosine kinase inhibitor PP2 at a concentration of 10 μM before incubation with DNP-albumin. Cells treated for 60 min with 10 μM PP3 were used as controls.

Flow cytometry analysis of FcεRI

To determine the surface FcεRI expression, cells (5×10^5/ml) were exposed for 30 min on ice to 1 μg/ml anti-DNP IgE followed by 30 min incubation with FITC-conjugated anti-mouse Ab (cross-reacting with mouse IgE). After incubation the cells were washed in ice-cold BSS-BSA. Mean fluorescence intensities were determined in the FL1 channel of FACSCalibur (BD Biosciences, Mountain View, CA).

Degranulation assay

The degree of degranulation was quantified as the release of β-glucuronidase from anti-DNP IgE-sensitized and DNP-albumin or thapsigargin-activated cells, using 4-methylumbelliferyl β-D-glucuronide as a substrate (27). The total content of the enzyme was evaluated in supernatants from cells lysed by 0.1% Triton X-100.

Determination of intracellular Ca^{2+} concentrations and $^{45}Ca^{2+}$ uptake

Concentrations of free intracellular calcium ($[Ca^{2+}]_i$) were determined using Fluo3 as a reporter. Cells were sensitized with anti-DNP IgE (1 μg/ml) at 37°C in culture medium supplemented with 10% FCS, but devoid of SCF and IL-3. After 4 h, the cells were washed and resuspended at a concentration of 1×10^7 cells/ml in the same medium supplemented with Fluo3 and probenecid at final concentrations of 1 μg/ml and 2.5 mM, respectively. After 30 min, the cells were washed in BSS-BSA supplemented with probenecid and put on ice for 10 min. Before measurement, the cells (5×10^5) were briefly centrifuged, resuspended in 200 μl BSS-BSA, and preincubated for 4 min at 37°C. Cells were activated by adding 100 ng/ml DNP-albumin or 2 μM thapsigargin. Calcium mobilization was determined in the FL1 channel of a FACSCalibur Flow Cytometer (BD Biosciences, San Jose, CA) using FlowJo software (Ashland, OR). In the yellow fluorescent protein (YFP)-hSTIM1 rescue experiments, calcium responses were measured 48 h after nucleofection. STIM1 KD cells nucleofected with pYFP alone (Clontech Laboratories, Mountain View, CA) were used as a mock control. The experimental procedure was similar to that described above with some differences. Cells were loaded with the calcium reporter Fura Red (5 μg/ml), and changes in fluorescence intensity were monitored on an LSRII flow cytometer (BD Biosciences). Populations of live cells were selected based on forward and side scatters. In live nucleofected cells, YFP-positive cells were gated based on fluorescence in the FL1 channel. Fura Red was excited with 406- and 488-nm lasers, and data were collected separately using 675/45 BP and 675/20 BP filters, respectively.

Uptake of extracellular calcium was determined as described previously (28). Cells were sensitized with anti-DNP IgE (1 μg/ml) and activated for various time intervals with 100 ng/ml DNP-albumin or 2 μM thapsigargin in the presence of extracellular $^{45}Ca^{2+}$ (1 mM). Cell-bound radioactivity was measured in 10 ml scintillation liquid (EcoLite; ICN Biomedicals, Costa Mesa, CA) using a QuantaSmart TM counter.

Chemotaxis assay

Chemotactic responses of BMMCs were examined using 96-well chemotaxis plates (ChemoTx system; Neuro Probe, Gaithersburg, MD) with 8-μm pore size polycarbonate filters. Chemoatractant (DNP-BSA) at concentrations of 50–250 ng/ml in RPMI 1640 supplemented with 20 mM HEPES and 1% BSA (assay buffer), or assay buffer alone was added in 305 μl to the lower wells, and IgE-sensitized BMMCs (0.15×10^6) in 60-μl assay buffer were added on top of the membrane above each well. After 8 h incubation at 37°C and 5% CO_2 in humidified air, cells on the upper membrane surface were removed with suction, and the plates with membrane frames were centrifuged ($156 \times g$, 4 min). After centrifugation, 200 μl media above the cells was removed and 100 μl of water containing 0.1% Triton X-100 and 10 μM SYTOX Green nucleic acid stain (Invitrogen) was added to the well. Fluorescence was determined at 485-nm excitation and 530-nm emission, using TECAN Infinite M200 fluorescence microplate reader (Grödig, Austria). A linear standard curve with serial dilutions of the cells (400–50,000 cells) was included in each experiment to equate fluorescence intensity with cell number. Four independent experiments were run in triplicates.

Gel electrophoresis and immunoblotting

Whole-cell extracts were prepared by washing the cells in cold PBS, solubilizing them in hot SDS-sample buffer (29), and boiling for 5 min. SDS-PAGE on 7.5% gels, electrophoretic transfer of separated proteins onto nitrocellulose, and details of the immunostaining procedure have been described elsewhere (30). Abs against STIM1 and actin were diluted 1:2000 and 1:3000, respectively. Bound primary Abs were detected after incubation of the blots with HRP-conjugated secondary Ab diluted 1:10,000. Phosphotyrosine was detected by PY-20–HRP conjugate (dilution 1:2000). HRP signal was detected with chemiluminescence reagents in accordance with the manufacturer's directions and quantified using LAS 3000 imaging system (Fujifilm, Tokyo, Japan).

Immunofluorescence microscopy

Immunofluorescence microscopy was performed on fixed cells as described previously (31). Cells attached to fibronectin-coated coverslips were rinsed with microtubule-stabilizing buffer (0.1 M MES, pH 6.9, 2 mM EGTA, 2 mM $MgCl_2$, 4% polyethylene glycol 6000), fixed for 20 min in 3% formaldehyde in microtubule-stabilizing buffer, and extracted for 4 min with 0.5% Triton X-100 in microtubule-stabilizing buffer. TUB 2.1 mAb conjugated with Cy3 and polyclonal Ab to α-tubulin were diluted 1:600 and 1:200, respectively. AlexaFluor 488-conjugated anti-rabbit Ab was diluted 1:300. The preparations were mounted in MOWIOL 4-88 (Merck, Darmstadt, Germany), supplemented with DAPI to label nuclei, and examined with an Olympus A70 Provis microscope equipped with ×60 water-immersion or ×100 oil-immersion objectives. Images were recorded with a SensiCam cooled CCD camera (PCO IMAGING, Kelheim, Germany). Conjugated secondary Ab did not give any detectable staining.

Alternatively, samples were examined with a confocal laser scanning microscope Leica TCS SP5 equipped with an ×63/1.4.N.A. oil-immersion objective. Excitation and emission wavelengths were 561 nm and 566 to 633 nm for Cy3 (diode pumped solid-state laser). Optical sections were acquired in 125-nm steps, and z-series were made from 70 sections. Deconvolution and rotation was performed using Huygens Deconvolution Software (Scientific Volume Imaging, Hilversum, The Netherlands).

To estimate the number of cells that responded to activation events by generation of microtubule protrusions, three independent immunofluorescence experiments were performed. In each experiment usually 500 cells were examined, and cells with five and more microtubule protrusions after activation were counted up. These protrusions were not discernible in nonactivated cells. Statistical comparison of data was conducted with Student *t* test.

Time-lapse imaging by total internal reflection fluorescence microscopy

Control BMMCL cells, BMMCL cells with empty pLKO.1 vector, or cells with STIM1 KD were nucleofected with pEB1-GFP. Alternatively, BMMCL cells were nucleofected with YFP-hSTIM1 or simultaneously with YFP-hSTIM1 and EB3-mRFP1. Twenty-four hours later, 100 μl of cell suspension at concentration 1.5×10^6 cells/ml was overlaid on 35-mm glass-bottom culture dishes (MatTek, Ashland, MA; Cat. No. P35G-1.5-14-C) precoated with fibronectin (see above), and cells were allowed to attach for 1 h at 37°C. Perfusion insert for the 35-mm culture dish was

Downloaded from www.jimmunol.org on December 22, 2010

inserted (Warner Instruments, Hamden, CT; model RC-37F), and cells were washed and subsequently incubated in RPMI medium for live cell imaging (RPMI 1640 without phenol red, riboflavin, folic acid, pyridoxal, $Fe[NO_3]_3$) supplemented with 20 mM HEPES. Cells were imaged on the Leica AM total internal reflection fluorescence (TIRF) MC (Leica Microsystems) at 37°C. Time-lapse sequences of EB1-GFP or YFP-hSTIM1 were acquired in TIRF mode (GFP cube, laser line 488 nm; Ex, 470/40; Em, 525/50; penetration depth, 150 nm) using HCX PL APO ×100/1.46 NA oil-immersion TIRF objective. Images were taken for 3 min at 1-s intervals with 30–40% laser power and exposure times ranging from 500–800 ms. Time-lapse sequences of EB3-mRFP1 in combination with YFP-hSTIM1 were acquired in TIRF mode (laser lines 561 nm or 488 nm, Em: 640/40 or 530/30, respectively; the same penetration depth 150 nm for both channels) using the same objective as above. Individual channels were imaged sequentially. Images were taken for 3 min at 2-s intervals with 50–80% (561 nm) or 30–40% (488 nm) laser power and exposure times ranging from 500–800 ms. Cells were scanned before, during, and after thapsigargin or nocodazole addition to final concentrations of 2 μM and 10 μM, respectively.

Time-lapse sequences were adjusted and analyzed with a particle tracking plug-in written in house. The images were smoothed to remove noise (σ 80 nm). The particles were then enhanced by subtracting the images obtained by Gaussian smoothing (σ 300 nm). The coordinates of particles were detected as centers of mass of maxima of the image intensity found by morphologic reconstruction (32). Regions of pixels with distance less than 3 μm from cell boundary were detected by thresholding the Euclidean distance transform (33) of the cell binary image. Only the particles in the selected region were evaluated. The corresponding particles in subsequent images were detected by pairing the closest particles, and the particle trajectories were constructed by continuation. The speed of the particles was calculated as the ratio of particle trajectory length and trajectory duration. The histogram of the particles speed was calculated from the trajectory speed weighted by the trajectory duration. The algorithms were implemented as plug-in modules of the Ellipse program, version 2.07 (ViDiTo, Systems, Košice Slovakia). Statistical analysis was done in Microsoft Excel.

Results

Reorganization of microtubules during activation of BMMCs

To compare microtubule organization in resting and activated mast cells, BMMCs were attached to fibronectin-coated coverslips and then activated by various means before fixation and immunofluorescence labeling for β-tubulin. Data showed a clear difference between resting and activated cells in microtubule distribution. Quiescent cells were characterized by rounded morphology and microtubules in cell periphery running predominantly alongside the plasma membrane (Fig. 1*A*, *a*, *b*; −Ag). When activated by FcεRI aggregation, many cells had multiple protrusions containing microtubules, in the following text denoted as microtubule protrusions (Fig. 1*A*, *c*, *d*; +Ag). Similarly, activation by pervanadate, a potent protein tyrosine phosphatase inhibitor (34) that mimics in part the stimulatory effect of Ag (35), gave rise to multiple microtubule protrusions (Fig. 1*A*, *e*, *f*; +Pv). Surprisingly, generation of robust microtubule protrusions was also found in cells treated with thapsigargin, a compound that discharges intracellular Ca^{2+} stores by inhibition of the SERCA (36) (Fig. 1*A*, *g*, *h*; +thapsigargin [Tg]). Microtubule protrusions do not reflect only the spreading of cells during activation events, because they are also found on the dorsal side of cells as clearly documented on deconvoluted three-dimensional images from laser scanning confocal microscopy. Although no protrusions were found in resting cells (Fig. 2*A*, 2*B*, –Ag), they were clearly discernible in cells activated by Ag-mediated FcεRI aggregation (Fig. 2*C*, 2*D*, +Ag), pervnadate (Fig. 2*E*, 2*F*, +Pv) or thapsigargin (Fig. 2*G*, 2*H*, +Tg). To determine whether the number of cells with protrusions depends on the mode of activation, BMMCs were evaluated for the presence of protrusions in three independent experiments (each included 500 cells). Activation of the cells with Ag, pervanadate, or thapsigargin resulted in 37 ± 9, 59 ± 8, and 94 ± 3%

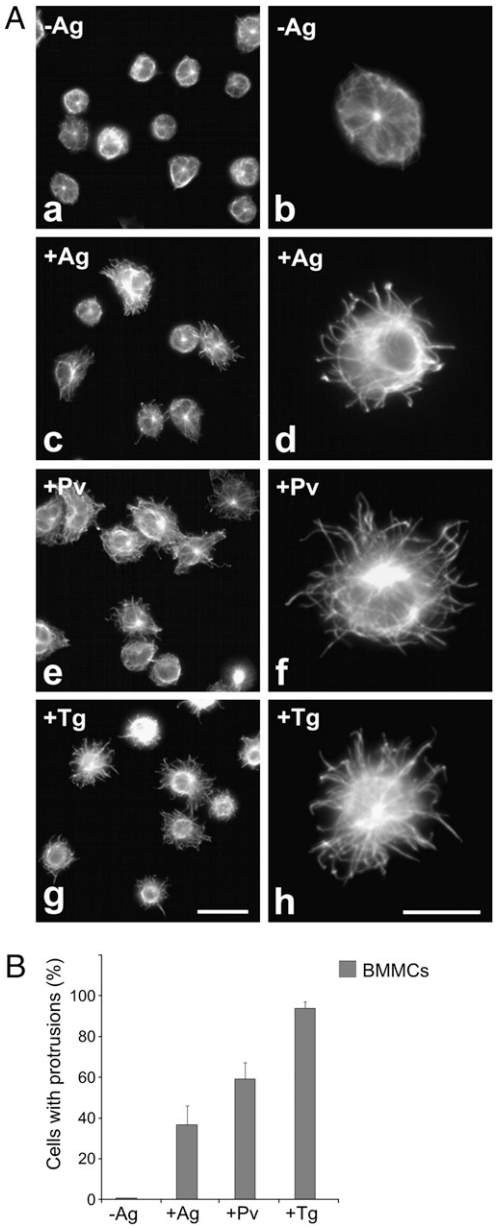

FIGURE 1. Organization of microtubules in resting and activated mast cells. *A*, Resting BMMCs (*a*, *b*; −Ag), the cells activated by FcεRI aggregation (*c*, *d*; +Ag), pervanadate (*e*, *f*; +Pv), or thapsigargin (*g*, *h*; +Tg) were fixed and stained for β-tubulin. The preparations were imaged by fluorescence microscopy. Scale bars, 20 μm (*g*) and 10 μm (*h*). Comparable magnifications are in (*a*, *c*, *e*, *g*) and in (*b*, *d*, *f*, *h*). *B*, Quantitative analysis of the frequency of microtubule protrusions in BMMCs. Resting cells (−Ag), cells activated by FcεRI aggregation (+Ag), pervanadate (+Pv) or thapsigargin (+Tg). Three independent experiments were performed, each involving 500 BMMCs examined for the presence of microtubule protrusions. Values indicate means ± SD (n = 3).

(mean ± SD; n = 3), respectively, of cells with microtubule protrusions (Fig. 1*B*). To prove that the generation of microtubule protrusion is not restricted only to cells of primary cultures, activations were repeated with an established cell line, BMMCL. In that case the rates of activation with Ag, pervanadate, or thapsigargin were 55 ± 10, 64 ± 3, and 80 ± 5% (mean ± SD; n = 3), respectively. The microtubule protrusions in cells activated by FcεRI aggregation were most prominent ~5 min after crosslinking. In contrast, cells stimulated by pervanadate or thapsigargin reached the maximum after 15 and 20 min, respectively.

Downloaded from www.jimmunol.org on December 22, 2010

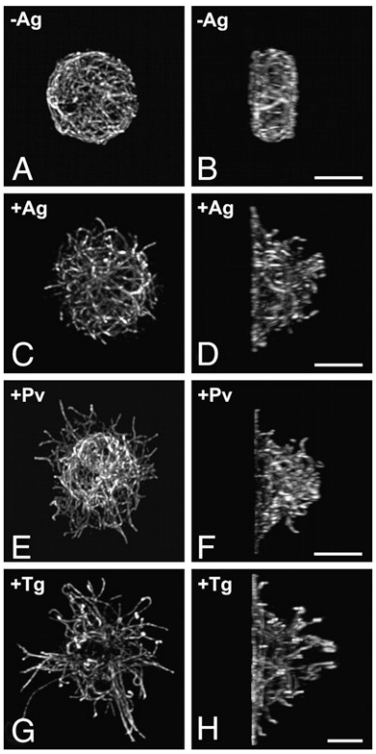

FIGURE 2. Changes in the spatial distribution of microtubules in resting and activated BMMCs. Resting cells (*A*, *B*; −Ag), cells activated by FcεRI aggregation (*C*, *D*; +Ag), pervanadate (*E*, *F*; +Pv), or thapsigargin (*G*, *H*; +Tg) were fixed and stained for β-tubulin. The preparations were imaged by laser scanning confocal microscopy. The stacks of confocal sections were deconvoluted and subjected to three-dimensional reconstruction. Resulting three-dimensional images viewed from top of the cells (*A*, *C*, *E*, *G*) and from the plane perpendicular to the plane of cell adhesion (*B*, *D*, *F*, *H*). Each pair (*A–B*, *C–D*, *E–F*, and *G–H*) represents the same cells. Scale bars, 5 μm.

Dose response curves demonstrating the relations between the formation of microtubule protrusions and the degree of degranulation, quantified as the release of β-glucuronidase, in BMMCL activated by FcεRI aggregation for 5 min and by thapsigargin for 20 min are shown in Supplemental Fig. 1A and 1B, respectively. There were dose response correlations between formation of microtubule protrusions and degranulation. Correlations between the time course of microtubule protrusion formation and the degree of degranulation after activation by FcεRI aggregation at Ag concentration 100 ng/ml and by thapsigargin at concentration 2 μM are shown in Supplemental Fig. 1C and 1D, respectively. Although there was a correlation between morphologic changes and degranulation in case of thapsigargin activation, cells activated by Ag reached the maximum of microtubule protrusions at 5 min, whereas the increase in β-glucuronidase release persisted to 10 min. Activation by either pervanadate or thapsigargin had no effect on viability of the cells (not shown). When the cells were pretreated with microtubule inhibitor nocodazole and activated in its presence, protrusions were not formed (not shown). This implies that microtubules are essential in this process.

Formation of microtubule protrusions in FcεRI-activated cells was substantially reduced if a monovalent hapten causing receptor disengagement (50 μM DNP-lysine) (37) was added together with or 1 min after Ag (not shown). Inhibition of protrusion formations was also observed in IgE-sensitized cells pretreated for 60 min with Src family inhibitor PP2 (10 μM) and then activated by Ag. Pretreatment with PP3 (negative control for PP2) failed to affect protrusion formation (not shown). This finding suggests that the activity of Src family protein tyrosine kinases is essential for this process. Interestingly, when the cells were activated by FcεRI aggregation, pervanadate, or thapsigargin in Ca^{2+}-free media, microtubule protrusions were basically not detectable. A typical example of the effect of extracellular Ca^{2+} on generation of microtubule protrusions in cells after their activation by FcεRI aggregation is shown in Fig. 3*A*. Statistical evaluation of these and other experiments is documented by histogram (Fig. 3*B*). Collectively, these data suggest that dramatic changes in microtubule arrangement during activation of BMMCs by FcεRI aggregation depend on the activity of Src family kinases and are modulated by Ca^{2+} influx.

Changes of microtubule dynamics in activated cells

Microtubule plus-end dynamics in BMMCL cells expressing EB1-GFP was monitored by means of time-lapse imaging using TIRF microscopy (TIRFM). Cells were activated or not by thapsigargin, and the distribution of growing microtubules in cell periphery was evaluated after collecting 180 frames in 1-s intervals for 3 min total time. In activated cells, time-lapse imaging started 13 min after thapsigargin addition. Data from a typical experiment are shown in Fig. 4*A*. A comparison of single-frame or 20-frame projections obtained either from control (Fig. 4*A*, *a*, *b*; –Tg) or thapsigargin-activated (Fig 4A, *c*, *d*; + Tg) cell indicated more growing microtubules in cell periphery of the latter. This finding was confirmed by statistical data evaluation and documented with

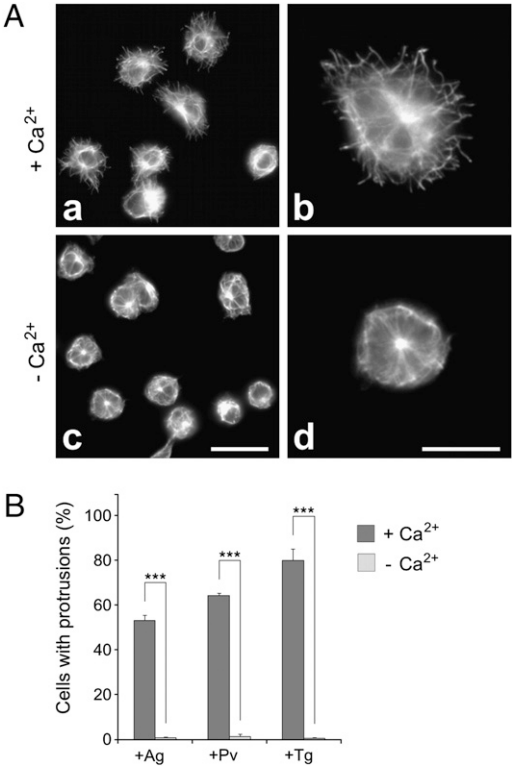

FIGURE 3. Effect of extracellular Ca^{2+} on generation of microtubule protrusions. *A*, BMMCL cells activated by FcεRI aggregation in the presence (*a*, *b*; $+Ca^{2+}$) or absence (*c*, *d*; $-Ca^{2+}$) of extracellular Ca^{2+} (1.8 mM) were fixed and stained for β-tubulin. Scale bars, 20 μm (*c*) and 10 μm (*d*). Comparable magnifications are in (*a*, *c*) and in (*b*, *d*). *B*, Statistical analysis of the frequency of microtubule protrusions in BMMCL cells. Cells activated by FcεRI aggregation (+Ag), pervanadate (+Pv), or thapsigargin (+Tg) in the presence ($+Ca^{2+}$) or absence ($-Ca^{2+}$) of extracellular Ca^{2+}. Three independent experiments were performed, each involving 500 cells, and examined for the presence of microtubule protrusions. Values indicate means ± SD, $n = 3$; ***$p < 0.001$.

Downloaded from www.jimmunol.org on December 22, 2010

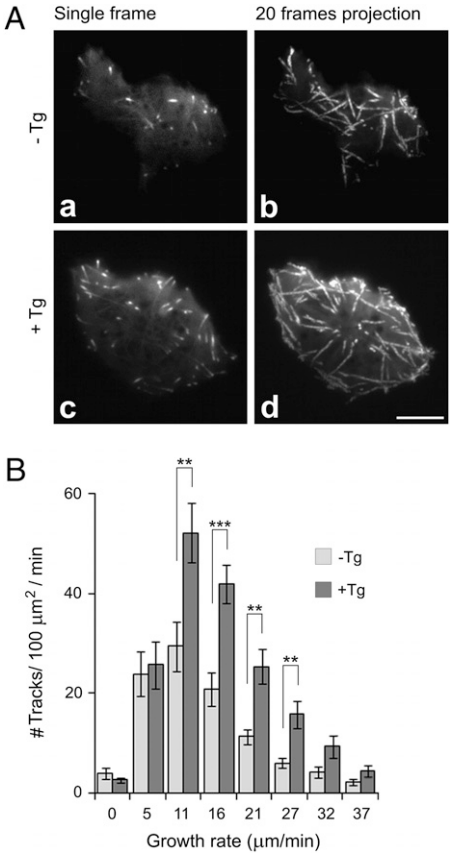

FIGURE 4. Activation of mast cells increases the number of growing microtubules in cell periphery as determined by TIRFM time-lapse imaging. *A*, Time-lapse imaging of resting (*a*, *b*) and thapsigargin-activated (*c*, *d*) BMMCL cells expressing EB1-GFP. Still images of EB1 (*a*, *c*) and tracks of EB1 comets over 20 s created by maximum intensity projection of the 20 consecutive frames (*b*, *d*). Scale bar, 5 μm. *B*, Histogram of microtubule growth rates in cell periphery of resting (−Tg) and thapsigargin-activated (+Tg) cells. A total of 15 different cells were tracked in five independent experiments. Values indicate mean ± SE, $n = 15$; $^{**}p < 0.01$; $^{***}p < 0.001$.

a histogram of the microtubule growth rates (Fig. 4*B*). Typical time-lapse imaging of control (Supplemental Video 1) and activated (Supplemental Video 2) cells are shown in the supplemental material. These data suggest that activation increases the number of growing microtubules in the cell periphery where microtubule protrusions are formed. More growing microtubules at cell periphery, compared with nonactivated cells, were also observed after activation of cells by FcεRI aggregation (Supplemental Fig. 2).

Reduced degranulation, Ca^{2+} influx, and free cytoplasmic Ca^{2+} concentration in cells with reduced level of STIM1

STIM1 represents the key regulator in the SOCE pathway leading to an influx of extracellular Ca^{2+}. To discover whether STIM1 is involved in the generation of microtubule protrusion, we first isolated cells with reduced levels of STIM1 and characterized their properties. STIM1-deficient cells were produced in both BMMCs and BMMCL cells using lentiviral vectors. At the best silencing, the amount of STIM1 in BMMCs and BMMCL cells reached 20 ± 12% and 10 ± 9% (means ± SD; n = 5-8), respectively, when compared with the expression level in control cells with an empty pLKO.1 vector. A typical immunoblotting experiment is shown in Fig. 5*A*, and evaluation of all data obtained is shown in Fig. 5*B*. Cells with the highest STIM1 reduction (denoted KD2) were selected for further experiments. As detected by flow cytometry, the

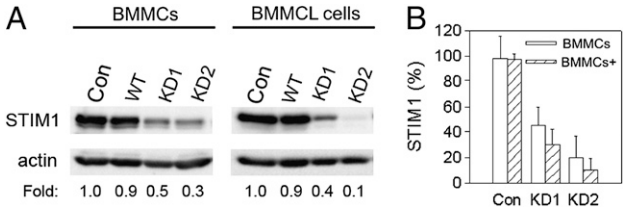

FIGURE 5. Characterization of mast cells with reduced level of STIM1. *A*, Immunoblots of whole cell lysates from BMMCs or BMMCL cells probed with anti-STIM1 and anti-actin (loading control) Abs. Control cells infected with empty pLKO.1 vector (Con), noninfected wild-type cells (WT), cells selected after KD of STIM1 by shRNA1 (KD1), or shRNA2 (KD2). Numbers under the blots indicate relative amounts of STIM1 normalized to control cells (Con) and to the amount of actin in individual samples (Fold). *B*, Comparison of STIM1 expression levels in control and STIM1 KD BMMCs or BMMCL cells. Values indicate means ± SD from independent experiments (n = 6 for controls; n = 3 for KD1; n = 5 for KD2).

expression levels of surface FcεRI were similar in cells with normal and reduced amount of STIM1 (not shown). No substantial changes in the profile of total tyrosine-phosphorylated proteins were detected in STIM1 KD2 cells (not shown).

It is well established that an increase in $[Ca^{2+}]_i$ is a prerequisite for mast cell degranulation (1). To confirm the functional relevance of STIM1 KD, we determined the degree of degranulation by measuring the release of β-glucuronidase in cells activated by FcεRI aggregation or by thapsigargin. As expected, a substantial decrease in degranulation was observed in BMMCs with STIM1 KD compared with control cells. The inhibition of degranulation was observed in cells activated by both FcεRI aggregation (Supplemental Fig. 3*A*) and by thapsigargin (Supplemental Fig. 3*B*). The uptake of $^{45}Ca^{2+}$ after activation by FcεRI aggregation (Supplemental Fig. 3*C*) or by thapsigargin (Supplemental Fig. 3*D*) was also inhibited in STIM1 KD cells. Finally, a substantially lower concentration of free intracellular calcium $[Ca^{2+}]_i$ was detected in STIM1 KD cells, after activation by both FcεRI aggregation (Supplemental Fig. 3*E*) and thapsigargin (Supplemental Fig. 3*F*; thapsigargin). Similar results were obtained with BMMCL cells (not shown). Collectively, these data clearly demonstrate that STIM1 is essential for Ca^{2+} mobilization and degranulation in cells used in this study.

Generation of microtubule protrusions is dependent on STIM1

When BMMCs carrying empty pLKO.1 vector were activated with thapsigargin, the formation of microtubule protrusions was prominent (Fig. 6*A*, *a*, *c*; control + Tg) and essentially the same as in BMMCs without vector (not shown). Alternatively, thapsigargin-induced activation in BMMCs with STIM1 KD failed to generate microtubule protrusions, and the cell shape was spherical (Fig. 6*A*, *b*, *d*; STIM1 KD + Tg). Significant inhibition of protrusion formations in STIM1 KD cells was also found after stimulation with pervanadate or Ag in both BMMCs and BMMCL cells (Fig. 6*B*). No obvious change in microtubule dynamics was detected by time-lapse imaging in BMMCL cells with STIM1 KD after activation by thapsigargin. Data from a typical experiment of time-lapse imaging are shown in Fig. 7*A*. Comparison of still images (single frame or 20 frames projections) from nonactivated (Fig. 7*A*, *a*, *b*; STIM1 KD – Tg) or activated (Fig 7A, *c*, *d*; STIM1 KD + Tg) cells disproved the notion that more microtubules grow in the cell periphery of activated cells. This finding was confirmed by the histogram comparing microtubule growth rates (Fig 7*B*). Although thapsigargin-activated cells exhibited some increase in the number of growing microtubules in the cell periphery, it was insignificant except for the fast-growing group (27 μm/min). In control

Downloaded from www.jimmunol.org on December 22, 2010

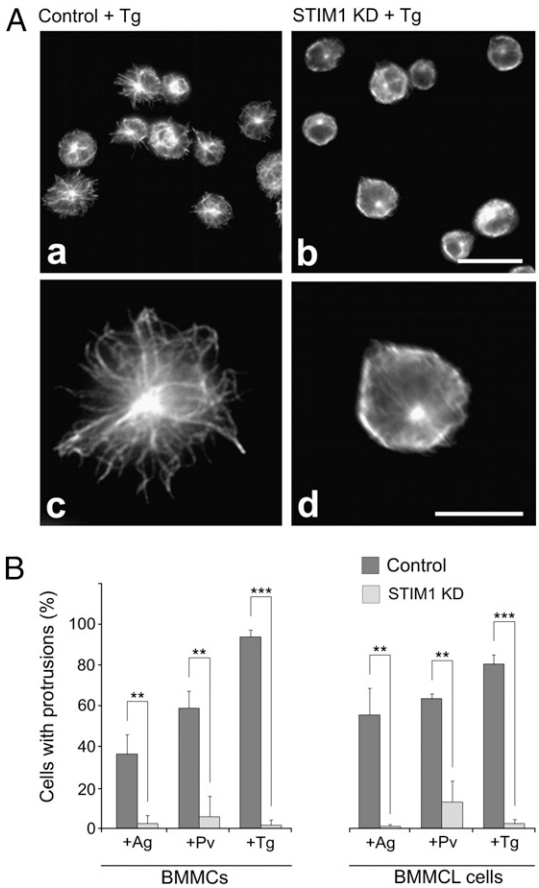

FIGURE 6. Decreased expression of STIM1 inhibits the generation of microtubule protrusions in activated cells. *A*, Control BMMCs, carrying empty pLKO.1 vector (*a*, *c*) or STIM1 KD2 cells (*b*, *d*) were activated by thapsigargin, fixed, and stained for β-tubulin. Scale bars, 20 μm (*a*, *b*) and 10 μm (*c*, *d*). *B*, Statistical analysis of the frequency of microtubule protrusions in control cells (carrying empty pLKO.1 vector) and STIM1 KD2 cells activated by FcεRI aggregation (+Ag), pervanadate (+Pv), or thapsigargin (+Tg). Three independent experiments were performed, each involving 500 BMMCs or BMMCL cells, and examined for the presence of microtubule protrusions. Values indicate means ± SD, $n = 3$; $^{**}p < 0.01$; $^{***}p < 0.001$.

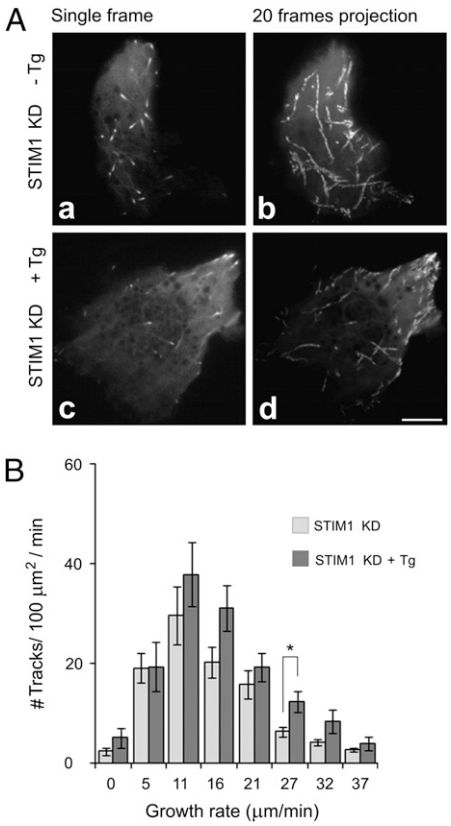

FIGURE 7. KD of STIM1 prevents changes in microtubule dynamics in activated cells as determined by TIRFM time-lapse imaging. STIM1 KD2 cells were nucleofected with EB1-GFP and used for time-lapse imaging. *A*, Resting (*a*, *b*) and thapsigargin-activated (*c*, *d*) STIM1 KD2 cells. Still images of EB1 (*a*, *c*) and tracks of EB1 comets over 20 s created by a maximum intensity projection of 20 consecutive frames (*b*, *d*). Scale bar, 5 μm. *B*, Histogram of microtubule growth rates in the cell periphery of resting (STIM1 KD) and thapsigargin-activated (STIM1 KD +Tg) cells. A total of nine different cells were tracked in three independent experiments. Values indicate means ± SE, $n = 9$; $^{*}p < 0.05$.

BMMCL cells carrying empty pLKO.1 vector, the distribution of growing microtubules in resting and thapsigargin-treated cells was similar as in BMMCL cells (Fig. 4).

To strengthen the evidence of STIM1-dependent formation of microtubule protrusions during activation, a rescue experiment was performed with construct-encoding mCherry-tagged human STIM1. Proper localization of mCherry-hSTIM1 was demonstrated in cells expressing EB1-GFP. It has been shown previously that STIM1 associates with the plus ends of growing microtubules (11); in addition, the mCherry-hSTIM1 localized in quiescent cells both in the ER and in the growing ends of microtubules labeled with EB1 (Fig. 8*A*, *a–c*). When BMMCL cells with STIM1 KD were nucleofected with mCherry-hSTIM1 and activated by thapsigargin, the formation of typical microtubule protrusions was recovered (Fig. 8*B*, *a–c*). Alternatively, no protrusions were generated after activation of cells nucleofected with empty mCherry vector (Fig. 8*B*, *d–f*). Control experiments revealed that no microtubule protrusions were evident in nonactivated BMMCL cells nucleofected either with mCherry-hSTIM1 or mCherry vector alone (not shown). The formation of microtubule protrusions was also recovered when YFP-hSTIM1 was used in rescue experiments as documented by quantitative data (Fig. 8*C*). Nucleofection of YFP-hSTIM1 into STIM1 KD2 cells also restored calcium mobilization upon triggering with thapsigargin (Fig. 8*D*) or aggregation of the FcεRI (not shown). Collectively, these data strongly suggest that STIM1 is essential for the generation of microtubule protrusions during activation of BMMCs.

Microtubules are not essential for STIM1 puncta formation

To address the question of whether microtubules in BMMCs have a role in activating SOCE, we investigated the effect of nocodazole, a microtubule-depolymerizing drug, on the distribution of STIM1 in the absence or presence of thapsigargin. In control cells, a typical comet-like movement was observed in quiescent BMMCs expressing YFP-hSTIM1 (Supplemental Video 3). After activation by thapsigargin, STIM1 formed puncta (Supplemental Video 4) similar to those previously described in other cells (5, 15). The addition of 10 μM nocodazole led to the rapid disappearance of comet-like movement of YFP-hSTIM1 as well as EB3-mRFP1, used as marker of growing microtubules. YFP-hSTIM1 was located only on the ER. When the nocodazole-treated cells were then activated with thapsigargin, YFP- hSTIM1 formed robust puncta (Supplemental Video 5). Staining of parallel samples for tubulin confirmed that most microtubules were disassembled (not shown). This finding suggests that initial STIM1 aggregation does not require intact microtubules. Interestingly, the disruption of microtubules only moderately inhibited the $^{45}Ca^{2+}$ uptake in

Downloaded from www.jimmunol.org on December 22, 2010

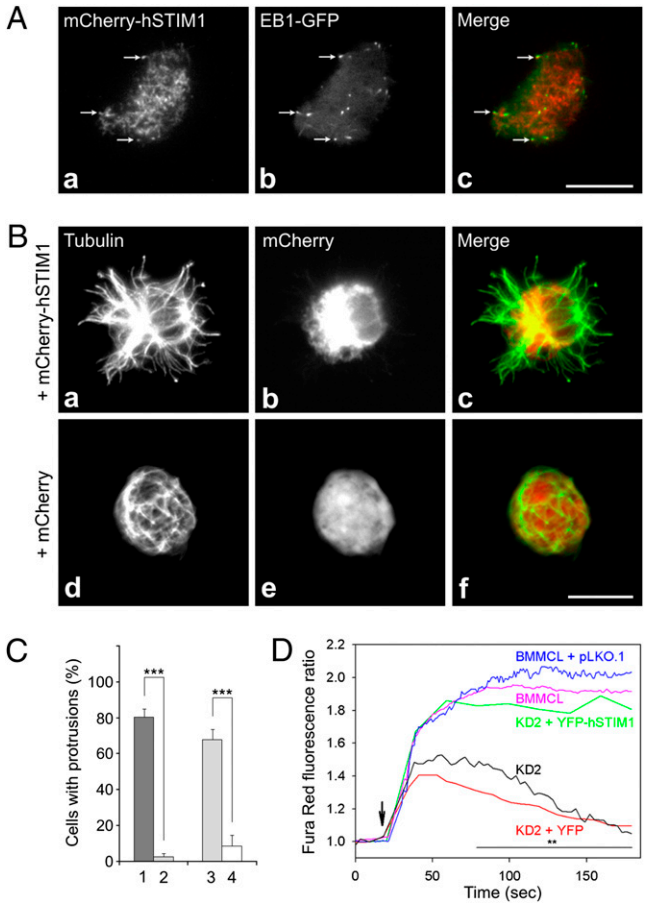

FIGURE 8. Phenotype rescue of STIM1 KD2 BMMCL cells after introduction of human STIM1. *A*, Localization of mCherry-tagged human STIM1 during TIRFM time-lapse imaging of resting cells expressing EB1-GFP. Still images of mCherry-hSTIM1 (*a*) EB1-GFP (*b*) and superposition of images (*c*; mCherry, red; GFP, green). Arrows indicate the same positions. Scale bar, 10 μm. *B*, STIM1 KD2 cells were nucleofected with mCherry-hSTIM1 (*a–c*) or mCherry vector alone (*d–f*; control) and activated by thapsigargin. Microtubules in fixed cells stained with anti-α-tubulin Ab (*a*, *d*). Fluorescence of nucleofected mCherry vectors (*b*, *e*). Superposition of images (*c*, *f*; tubulin, green; mCherry, red). The preparations were imaged by fluorescence microscopy; *a–c* and *d–f* represent the same cells. Scale bar, 10 μm. *C*, Statistical analysis of the frequency of microtubule protrusions in thapsigargin-activated control cells (1), STIM1 KD2 cells (2), STIM1 KD2 cells nucleofected with pYFP-hSTIM1 (3) and STIM1 KD2 cells nucleofected with pYFP empty vector (4). Three independent experiments were performed, each involving 500 (1, 2) or 100 (3, 4) cells examined for the presence of microtubule protrusions. Values indicate means ± SD, $n = 3$; $***p < 0.001$. *D*, Changes in intracellular Ca^{2+} mobilization. KD2 cells were nucleofected with pYFP-hSTIM1 (green line) or with pYFP empty vector (red line). Nontransfected cells (pink line), cells transfected with pLKO.1 (blue line) and STIM1 KD2 cells (black line) served as controls. The arrow indicates activation by 2 μM thapsigargin. The extent of activation is expressed as a ratio of Fura Red fluorescence intensity induced with 406- and 488-nm lasers. Representative curves are plotted against time. The line below the asterisks indicates the time interval of significant differences between STIM1 KD2 cell transfected with pYFP-hSTIM1 or with pYFP empty vector; $**p < 0.01$; $n = 3$.

thapsigargin-activated cells (Fig. 9*A*), but degranulation was substantially reduced (Fig. 9*B*).

STIM1 associates with microtubule protrusions and plays a role in chemotactic response

The movement of YFP-hSTIM1, not associated with growing tips of microtubules, was observable at later stages of activation when microtubule protrusions started to form. Association of YFP-hSTIM1 with microtubule protrusions was evident in thapsigargin-activated BMMCs and was detectable by confocal microscopy on cells stained for β-tubulin (Fig. 10*A*, *a–c*). Similarly, FcεRI aggregation led to partial association of YFP-hSTIM1 with microtubule protrusions (not shown).

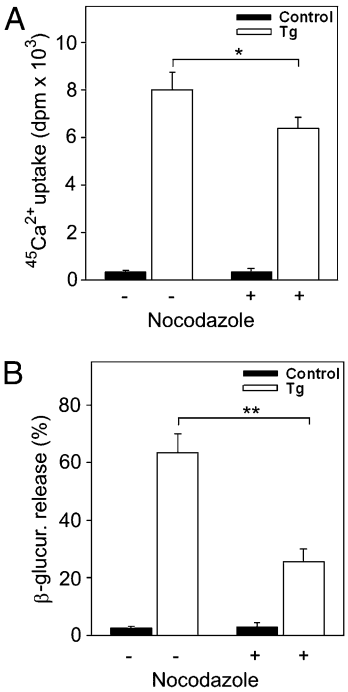

FIGURE 9. Effect of microtubule depolymerization on Ca^{2+} uptake and degranulation. *A*, Effect of nocodazole on Ca^{2+} uptake. BMMCs were treated or not with nocodazole (10 μM) for 30 min and then exposed to thapsigargin (2 μM; Tg) or BSS-BSA alone (Control) for 15 min in the presence of extracellular $^{45}Ca^{2+}$ (1 mM) and nocodazole (10 μM). *B*, Effect of nocodazole on degranulation. BMMCs were treated with nocodazole and exposed to thapsigargin as in *A*, and the release of β-glucuronidase was determined. Data in *A* and *B* represent means ± SD, $n = 6–8$; $*p < 0.05$; $**p < 0.01$.

The observed formation of STIM1-dependent microtubule protrusions could be related to enhanced movement of the activated cells. Therefore, in additional experiments, we investigated the chemotactic response of STIM1-deficient BMMCs. The data presented in Fig. 10*B* indicate that at low concentrations of Ag (25–100 ng/ml), the chemotactic response is contingent on STIM1 in a dose-dependent manner. At a higher concentration (250 ng/ml), the difference disappears mainly because of the high-dose–mediated inhibition of chemotaxis in control cells. This finding demonstrates that STIM1-dependent Ca^{2+} influx promotes chemotaxis.

Discussion

FcεRI stimulation of mast cells leads to rapid cytoskeleton rearrangement that is important for cell activation and degranulation. Accumulating recent data point to an important role of microtubules in these processes (38). Previous studies focused primarily on the role of microtubules in granular transport (13, 16, 17, 20) or on the initial stages of SOCE signaling pathway (13, 15, 39). In this study, we show that microtubule network rearrangement in activated BMMCs and formation of microtubule protrusions is dependent on the activity of Ca^{2+} sensor STIM1. This conclusion is supported by several lines of evidence. First, microtubule protrusions were found in cells stimulated by three types of activators that induced depletion of Ca^{2+} from internal stores (FcεRI aggregation, pervanadate, or thapsigargin treatment). Second, the generation of protrusions was impaired when multivalent Ag-

Downloaded from www.jimmunol.org on December 22, 2010

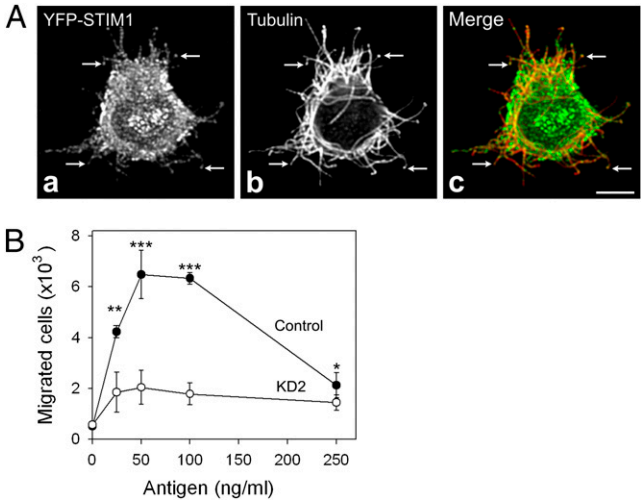

FIGURE 10. STIM1 associates with microtubule protrusions in activated cells and is essential for chemotactic response. *A*, Laser scanning confocal microscopy of BMMCL cells expressing YFP-hSTIM1 after activation by thapsigargin. Cells were fixed and immunostained for β-tubulin, and both STIM1 (*a*) and tubulin (*b*) were visualized in a single confocal section. Superposition of STIM1 and tubulin staining is shown in *c*. Association of YFP-hSTIM1 with microtubule protrusions is depicted (arrows). Scale bar, 5 μm. *B*, Chemotactic response in activated cells. Various concentrations of DNP-BSA (chemoattractant) were added to the lower wells of ChemoTx system plate, and IgE-sensitized BMMCs infected with empty pLKO.1 vector (Control) or STIM1 KD2 cells (KD2) were added on top of the membrane above each well. The numbers of cells migrated to the lower well were determined as described in *Materials and Methods*. Values indicate mean ± SD, $n = 12$; $*p < 0.05$; $**p < 0.01$; $***p < 0.001$.

induced FcεRI aggregation and signaling were inhibited either by monovalent hapten or by Src family specific inhibitor; this implies that early, physiologically relevant signaling events leading to STIM1 aggregation are important for microtubule rearrangement. Third, the formation of protrusions was also inhibited in cells with a decreased level of STIM1 and with correspondingly diminished influx of extracellular Ca^{2+}. Fourth, microtubule protrusions were restored in STIM1 KD cells after the introduction of hSTIM1. Finally, microtubule protrusions were not observed in cells activated in Ca^{2+}-free media. Thus, STIM1-regulated Ca^{2+} influx plays a crucial role in the generation of microtubule protrusions.

We have shown previously that, compared with resting cells, FcεRI- or pervanadate-induced activation of BMMCs attached to poly-L-lysine-coated coverslips resulted in more intense staining of microtubules. However, no obvious microtubule protrusions were detected (21). Similarly, activation and fixation of BMMCs in suspension followed by attachment to glass slides by cytospin intensified the tubulin immunostaining, but microtubule protrusions were not reported (17). In this study, the cells were attached to fibronectin before activation, resembling more closely the natural conditions in connective tissue where mast cells are congregated (40). Although the attachment of BMMCs to fibronectin alone did not generate microtubule protrusions, they were observable after cell triggering. It is known that engagement of integrins by their ligands activates some signaling pathways that modulate signals originating from other receptors (41). It has been reported that, when mast cells were activated simultaneously via both FcεRI and integrins, phosphorylation events were prolonged and intensified (42). Thus, generation of microtubule protrusions could reflect such integrated signals in activated cells.

To discover whether the generation of microtubule protrusions is limited to BMMCs, several other cell types were tested. However, thapsigargin treatment failed to induce formation of protrusions in any other cell type examined, including mouse embryonal fibroblasts 3T3, human osteosarcoma cell line U2OS or human glioblastoma T98G (Z. Hájková, unpublished data). By contrast, in BMMCL cells, which are grown for many years in the absence of SCF, the formation of protrusions was observed after triggering with cell activators (Ag, pervanadate, thapsigargin). The reduction of STIM1 expression both in BMMCs and BMMCL cells had a detrimental impact on the formation of microtubule protrusions. This finding indicates that protrusion formation could be a typical feature of mast cells that are characterized by immediate response to outer stimuli. However, we cannot rule out at present that the generation of microtubule protrusions can also be observable in the other cell types.

Colocalization of ER-embedded STIM1 with microtubules has been described for several cell types, including rat basophilic leukemia RBL-2H3 (8, 9, 15, 43), and comet-like movement of STIM1 was also reported (11). Furthermore, STIM1 contains a short sequence (SxIP) responsible for direct binding to EB1 (44). Thus, STIM1 can associate with growing microtubules, a mechanism that might facilitate the transport of STIM1 to plasma membrane. Using TIRFM we have confirmed the comet-like movement of STIM1 and its association with EB1 in resting BMMCL cells. This movement was substantially reduced after the addition of thapsigargin, which is in agreement with the impaired association of STIM1 with microtubules in Ag-activated RBL-2H3 cells (43). Recent data on FRET imaging of EB1 and STIM1 in HEK293 cells showed that, upon store depletion of Ca^{2+}, STIM1 dissociated from EB1 and associated with SERCA. This process was reversible, because the replenishment of intracellular Ca^{2+} stores also restored the STIM1–EB1 interactions (45). Moreover, no effect on SOCE was observed in HeLa cells with depleted EB1 (11). Taking these findings together, it is likely that the interaction of STIM1 with EB1 on growing microtubules is not essential for the transport of STIM1 to plasma membrane during mast cell activation.

After depletion of intracellular Ca^{2+} stores, STIM1 accumulates into puncta, discrete subregions of ER located in a close proximity (10–25 nm) to the plasma membrane (46). STIM1 puncta are formed several seconds before the opening of calcium channels (47), and one could expect that microtubules are involved in this process. However, our data demonstrate that although microtubule disruption by nocodazole abolished the comet-like movement of STIM1, it had no effect on puncta formation in activated cells. This finding is in line with our observation that the uptake of extracellular Ca^{2+} was only partially inhibited in nocodazole-pretreated and thapsigargin-activated BMMCs. This suggests that STIM1 aggregation beneath the plasma membrane and subsequent opening of Ca^{2+} release-activated Ca^{2+} channels does not require intact microtubules in activated mast cells. Previous studies often reported discordant effects of nocodazole treatment on SOCE or I_{CRAC}, the current most frequently associated with SOCE, in various cell types. Whereas there was no effect of nocodazole treatment observed in NIH 3T3 (48), RBL-1 (15, 39), and DT40 cells (8), an inhibitory effect was demonstrated for other cell types, such as RBL-2H3 cells, BMMCs (13), and HEK 293 (15). It appears that different factors, including cell type, treatment protocol and the way of Ca^{2+} depletion might modify the results of the experiments. It is also possible that microtubules play a supporting role in SOCE signaling by optimizing the location of ER containing STIM1 before cell activation (15).

Nocodazole treatment, on the other hand, effectively suppressed degranulation in BMMCs, suggesting that microtubules have a key role in the intracellular transport of granules. This finding is in accordance with previously published data demonstrating

Downloaded from www.jimmunol.org on December 22, 2010

microtubule-dependent movement of secretory vesicles during exocytotic response (16, 17, 20) and studies documenting a dramatic decrease in degranulation, but not in Ca^{2+} response in nocodazole treated cells (49). Our observation that STIM1 puncta are associated with microtubules in protrusions (Fig. 10*A*) indicates that microtubules might be important for translocation of clustered STIM1 as well. This process could possibly be dependent on the movement of ER components to protrusions via microtubule motor proteins; an important role of kinesin and dynein in the distribution of ER has already been reported (14).

Compared with quiescent cells or cells with decreased expression of STIM1, the number of growing microtubules at the periphery of activated BMMCL cells is substantially increased. This finding suggests the stabilization of microtubule plus ends. It is known that an important role in stabilization of growing microtubules is to be assigned to the plus end-tracking proteins whose interactions with microtubules are regulated by phosphorylation (10). Ca^{2+}-dependent kinases (e.g., conventional protein kinases C, calcium-calmodulin–dependent kinases) or phosphatases (e.g., PP2B) might participate in the regulation of microtubule stability in activated BMMCs. It has been reported that calcium-dependent activation of Rac (from the RhoA family of small GTPases) depends on the activity of conventional protein kinase C (50). FcεRI stimulation induced in BMMCs the activation of RhoA (17), which participates in the stabilization of microtubule plus ends through its target mDia (51). It remains to be determined whether stimulated kinases, small GTPases, or both have a stabilizing role in thapsigargin-treated BMMCs.

Nishida et al. (17) reported that FcεRI stimulation of BMMCs triggered the formation of microtubules and the translocation of granules in a manner independent of Ca^{2+}. Alternatively, our results demonstrate Ca^{2+}-dependent formation of microtubule protrusions. This discrepancy could be explained by differences in cell activation (the absence or presence of integrin engagement) and unlike methods of preparation of samples for microscopic evaluation, as discussed above. However, it is also possible that the initial stages of microtubule formation and transport of granules along microtubules are independent of Ca^{2+}, but later stages of activation and formation of microtubule protrusions depend on sustained influx of Ca^{2+}. The presence of aggregated STIM1 in protrusion could help to organize Ca^{2+} release-activated Ca^{2+} channels (46) and open locally these channels to cause SOCE. These interactions could be modulated by Ca^{2+} channel regulators, such as calmodulin (52) and the recently discovered CRACR2A (53). Our finding that STIM1-deficient BMMCs exhibited defective chemotaxis toward Ag is in line with these interpretations, and it supports previous data on the role of Ca^{2+} in chemotaxis (54, 55). We propose that microtubule protrusions might be involved in sensing external chemotactic gradients of Ag or other signals reaching mast cells at inflammatory sites.

In conclusion, our data indicate that the activation of mast cells leads to microtubule rearrangements and formation of microtubule protrusions. This process is dependent on STIM1-induced SOCE and enhanced levels of free cytoplasmic Ca^{2+} concentration, which have an important role in the regulation of microtubule dynamics, degranulation, and chemotactic response. Interference with the microtubular network via STIM1 or other Ca^{2+} regulators could potentially open new rational approaches to the treatment of inflammatory and allergic diseases.

Acknowledgments

We thank Dr. M. Hibbs (Ludwig Institute for Cancer Research, Melbourne, Australia) for BMMCL cells, Dr. T. Meyer (Department of Molecular Pharmacology, Stanford University Medical School, Stanford, CA) for YFP–hSTIM1 construct, Dr. Y. Mimori-Kiyosue (KAN Research Institute, Kyoto, Japan) for EB1-GFP construct, and Dr. A. Akhmanova (Department of Cell Biology, Erasmus Medical Center, Rotterdam, The Netherlands) for EB3-mRFP1.

Disclosures

The authors have no financial conflicts of interest.

References

1. Rivera, J., N. A. Fierro, A. Olivera, and R. Suzuki. 2008. New insights on mast cell activation via the high affinity receptor for IgE. *Adv. Immunol.* 98: 85–120.
2. Parekh, A. B., and J. W. Putney, Jr. 2005. Store-operated calcium channels. *Physiol. Rev.* 85: 757–810.
3. Smyth, J. T., W. I. Dehaven, B. F. Jones, J. C. Mercer, M. Trebak, G. Vazquez, and J. W. Putney, Jr. 2006. Emerging perspectives in store-operated Ca^{2+} entry: roles of Orai, Stim and TRP. *Biochim. Biophys. Acta* 1763: 1147–1160.
4. Roos, J., P. J. DiGregorio, A. V. Yeromin, K. Ohlsen, M. Lioudyno, S. Zhang, O. Safrina, J. A. Kozak, S. L. Wagner, M. D. Cahalan, et al. 2005. STIM1, an essential and conserved component of store-operated Ca^{2+} channel function. *J. Cell Biol.* 169: 435–445.
5. Liou, J., M. L. Kim, W. D. Heo, J. T. Jones, J. W. Myers, J. E. Ferrell, Jr., and T. Meyer. 2005. STIM is a Ca^{2+} sensor essential for Ca^{2+}-store-depletion-triggered Ca^{2+} influx. *Curr. Biol.* 15: 1235–1241.
6. Dziadek, M. A., and L. S. Johnstone. 2007. Biochemical properties and cellular localisation of STIM proteins. *Cell Calcium* 42: 123–132.
7. Prakriya, M., S. Feske, Y. Gwack, S. Srikanth, A. Rao, and P. G. Hogan. 2006. Orai1 is an essential pore subunit of the CRAC channel. *Nature* 443: 230–233.
8. Baba, Y., K. Hayashi, Y. Fujii, A. Mizushima, H. Watarai, M. Wakamori, T. Numaga, Y. Mori, M. Iino, M. Hikida, and T. Kurosaki. 2006. Coupling of STIM1 to store-operated Ca^{2+} entry through its constitutive and inducible movement in the endoplasmic reticulum. *Proc. Natl. Acad. Sci. USA* 103: 16704–16709.
9. Mercer, J. C., W. I. Dehaven, J. T. Smyth, B. Wedel, R. R. Boyles, G. S. Bird, and J. W. Putney, Jr. 2006. Large store-operated calcium selective currents due to co-expression of Orai1 or Orai2 with the intracellular calcium sensor, Stim1. *J. Biol. Chem.* 281: 24979–24990.
10. Akhmanova, A., and M. O. Steinmetz. 2008. Tracking the ends: a dynamic protein network controls the fate of microtubule tips. *Nat. Rev. Mol. Cell Biol.* 9: 309–322.
11. Grigoriev, I., S. M. Gouveia, B. van der Vaart, J. Demmers, J. T. Smyth, S. Honnappa, D. Splinter, M. O. Steinmetz, J. W. Putney, Jr., C. C. Hoogenraad, and A. Akhmanova. 2008. STIM1 is a MT-plus-end-tracking protein involved in remodeling of the ER. *Curr. Biol.* 18: 177–182.
12. Terasaki, M., L. B. Chen, and K. Fujiwara. 1986. Microtubules and the endoplasmic reticulum are highly interdependent structures. *J. Cell Biol.* 103: 1557–1568.
13. Oka, T., M. Hori, and H. Ozaki. 2005. Microtubule disruption suppresses allergic response through the inhibition of calcium influx in the mast cell degranulation pathway. *J. Immunol.* 174: 4584–4589.
14. Wu, S., H. Chen, M. F. Alexeyev, J. A. King, T. M. Moore, T. Stevens, and R. D. Balczon. 2007. Microtubule motors regulate ISOC activation necessary to increase endothelial cell permeability. *J. Biol. Chem.* 282: 34801–34808.
15. Smyth, J. T., W. I. DeHaven, G. S. Bird, and J. W. Putney, Jr. 2007. Role of the microtubule cytoskeleton in the function of the store-operated Ca^{2+} channel activator STIM1. *J. Cell Sci.* 120: 3762–3771.
16. Smith, A. J., J. R. Pfeiffer, J. Zhang, A. M. Martinez, G. M. Griffiths, and B. S. Wilson. 2003. Microtubule-dependent transport of secretory vesicles in RBL-2H3 cells. *Traffic* 4: 302–312.
17. Nishida, K., S. Yamasaki, Y. Ito, K. Kabu, K. Hattori, T. Tezuka, H. Nishizumi, D. Kitamura, R. Goitsuka, R. S. Geha, et al. 2005. FcεRI-mediated mast cell degranulation requires calcium-independent microtubule-dependent translocation of granules to the plasma membrane. *J. Cell Biol.* 170: 115–126.
18. Urata, C., and R. P. Siraganian. 1985. Pharmacologic modulation of the IgE or Ca^{2+} Ionophore A23187 mediated Ca^{2+} influx, phospholipase activation, and histamine release in rat basophilic leukemia cells. *Int. Arch. Allergy Immunol.* 78: 92–100.
19. Tasaka, K., M. Mio, K. Fujisawa, and I. Aoki. 1991. Role of microtubules on Ca^{2+} release from the endoplasmic reticulum and associated histamine release from rat peritoneal mast cells. *Biochem. Pharmacol.* 41: 1031–1037.
20. Martin-Verdeaux, S., I. Pombo, B. Iannascoli, M. Roa, N. Varin-Blank, J. Rivera, and U. Blank. 2003. Evidence of a role for Munc18-2 and microtubules in mast cell granule exocytosis. *J. Cell Sci.* 116: 325–334.
21. Sulimenko, V., E. Dráberová, T. Sulimenko, L. Macurek, V. Richterová, P. Dráber, and P. Dráber. 2006. Regulation of microtubule formation in activated mast cells by complexes of γ-tubulin with Fyn and Syk kinases. *J. Immunol.* 176: 7243–7253.
22. Oritani, K., and P. W. Kincade. 1996. Identification of stromal cell products that interact with pre-B cells. *J. Cell Biol.* 134: 771–782.
23. Nováková, M., E. Dráberová, W. Schürmann, G. Czihak, V. Viklický, and P. Dráber. 1996. γ-Tubulin redistribution in taxol-treated mitotic cells probed by monoclonal antibodies. *Cell Motil. Cytoskeleton* 33: 38–51.
24. Dráber, P., J. Zikán, and M. Vojtíšková. 1980. Establishment and characterization of permanent murine hybridomas secreting monoclonal anti-thy-1 antibodies. *J. Immunogenet.* 7: 455–474.

Downloaded from www.jimmunol.org on December 22, 2010

25. Mimori-Kiyosue, Y., N. Shiina, and S. Tsukita. 2000. The dynamic behavior of the APC-binding protein EB1 on the distal ends of microtubules. *Curr. Biol.* 10: 865–868.
26. Campbell, R. E., O. Tour, A. E. Palmer, P. A. Steinbach, G. S. Baird, D. A. Zacharias, and R. Y. Tsien. 2002. A monomeric red fluorescent protein. *Proc. Natl. Acad. Sci. USA* 99: 7877–7882.
27. Surviladze, Z., L. Dráberová, M. Kovářová, M. Boubelík, and P. Dráber. 2001. Differential sensitivity to acute cholesterol lowering of activation mediated via the high-affinity IgE receptor and Thy-1 glycoprotein. *Eur. J. Immunol.* 31: 1–10.
28. Dráberová, L. 1990. Cyclosporin A inhibits rat mast cell activation. *Eur. J. Immunol.* 20: 1469–1473.
29. Laemmli, U. K. 1970. Cleavage of structural proteins during the assembly of the head of bacteriophage T_4. *Nature* 227: 680–685.
30. Dráber, P., L. A. Lagunowich, E. Dráberová, V. Viklický, and I. Damjanov. 1988. Heterogeneity of tubulin epitopes in mouse fetal tissues. *Histochemistry* 89: 485–492.
31. Dráberová, E., and P. Dráber. 1993. A microtubule-interacting protein involved in coalignment of vimentin intermediate filaments with microtubules. *J. Cell Sci.* 106: 1263–1273.
32. Soile, P. 2003. *Morphological Image Analysis – Principles and Applications.* Springer Verlag, Berlin.
33. Breu, H., D. Kirkpatrick, and M. Werman. 1995. Linear time euclidean distance transform algorithms. *IEEE Trans. Pattern Anal. Mach. Intell.* 17: 529–533.
34. Zick, Y., and R. Sagi-Eisenberg. 1990. A combination of H_2O_2 and vanadate concomitantly stimulates protein tyrosine phosphorylation and polyphosphoinositide breakdown in different cell lines. *Biochemistry* 29: 10240–10245.
35. Teshima, R., H. Ikebuchi, M. Nakanishi, and J. Sawada. 1994. Stimulatory effect of pervanadate on calcium signals and histamine secretion of RBL-2H3 cells. *Biochem. J.* 302: 867–874.
36. Thastrup, O., P. J. Cullen, B. K. Drøbak, M. R. Hanley, and A. P. Dawson. 1990. Thapsigargin, a tumor promoter, discharges intracellular Ca^{2+} stores by specific inhibition of the endoplasmic reticulum Ca^{2+}-ATPase. *Proc. Natl. Acad. Sci. USA* 87: 2466–2470.
37. Paolini, R., M. H. Jouvin, and J. P. Kinet. 1991. Phosphorylation and dephosphorylation of the high-affinity receptor for immunoglobulin E immediately after receptor engagement and disengagement. *Nature* 353: 855–858.
38. Gilfillan, A. M., and J. Rivera. 2009. The tyrosine kinase network regulating mast cell activation. *Immunol. Rev.* 228: 149–169.
39. Bakowski, D., M. D. Glitsch, and A. B. Parekh. 2001. An examination of the secretion-like coupling model for the activation of the Ca^{2+} release-activated Ca^{2+} current I_{CRAC} in RBL-1 cells. *J. Physiol.* 532: 55–71.
40. Galli, S. J., M. Tsai, and A. M. Piliponsky. 2008. The development of allergic inflammation. *Nature* 454: 445–454.
41. Schwartz, M. A., M. D. Schaller, and M. H. Ginsberg. 1995. Integrins: emerging paradigms of signal transduction. *Annu. Rev. Cell Dev. Biol.* 11: 549–599.
42. Lam, V., J. Kalesnikoff, C. W. Lee, V. Hernandez-Hansen, B. S. Wilson, J. M. Oliver, and G. Krystal. 2003. IgE alone stimulates mast cell adhesion to fibronectin via pathways similar to those used by IgE + antigen but distinct from those used by Steel factor. *Blood* 102: 1405–1413.
43. Calloway, N., M. Vig, J. P. Kinet, D. Holowka, and B. Baird. 2009. Molecular clustering of STIM1 with Orai1/CRACM1 at the plasma membrane depends dynamically on depletion of Ca^{2+} stores and on electrostatic interactions. *Mol. Biol. Cell* 20: 389–399.
44. Honnappa, S., S. M. Gouveia, A. Weisbrich, F. F. Damberger, N. S. Bhavesh, H. Jawhari, I. Grigoriev, F. J. van Rijssel, R. M. Buey, A. Lawera, et al. 2009. An EB1-binding motif acts as a microtubule tip localization signal. *Cell* 138: 366–376.
45. Sampieri, A., A. Zepeda, A. Asanov, and L. Vaca. 2009. Visualizing the store-operated channel complex assembly in real time: identification of SERCA2 as a new member. *Cell Calcium* 45: 439–446.
46. Cahalan, M. D. 2009. STIMulating store-operated Ca^{2+} entry. *Nat. Cell Biol.* 11: 669–677.
47. Wu, M. M., J. Buchanan, R. M. Luik, and R. S. Lewis. 2006. Ca^{2+} store depletion causes STIM1 to accumulate in ER regions closely associated with the plasma membrane. *J. Cell Biol.* 174: 803–813.
48. Ribeiro, C. M., J. Reece, and J. W. Putney, Jr. 1997. Role of the cytoskeleton in calcium signaling in NIH 3T3 cells. An intact cytoskeleton is required for agonist-induced $[Ca^{2+}]i$ signaling, but not for capacitative calcium entry. *J. Biol. Chem.* 272: 26555–26561.
49. Hesketh, T. R., M. A. Beaven, J. Rogers, B. Burke, and G. B. Warren. 1984. Stimulated release of histamine by a rat mast cell line is inhibited during mitosis. *J. Cell Biol.* 98: 2250–2254.
50. Price, L. S., M. Langeslag, J. P. ten Klooster, P. L. Hordijk, K. Jalink, and J. G. Collard. 2003. Calcium signaling regulates translocation and activation of Rac. *J. Biol. Chem.* 278: 39413–39421.
51. Palazzo, A. F., T. A. Cook, A. S. Alberts, and G. G. Gundersen. 2001. mDia mediates Rho-regulated formation and orientation of stable microtubules. *Nat. Cell Biol.* 3: 723–729.
52. Mullins, F. M., C. Y. Park, R. E. Dolmetsch, and R. S. Lewis. 2009. STIM1 and calmodulin interact with Orai1 to induce Ca^{2+}-dependent inactivation of CRAC channels. *Proc. Natl. Acad. Sci. USA* 106: 15495–15500.
53. Srikanth, S., H. J. Jung, K. D. Kim, P. Souda, J. Whitelegge, and Y. Gwack. 2010. A novel EF-hand protein, CRACR2A, is a cytosolic Ca^{2+} sensor that stabilizes CRAC channels in T cells. *Nat. Cell Biol.* 12: 436–446.
54. Hartmann, K., B. M. Henz, S. Krüger-Krasagakes, J. Köhl, R. Burger, S. Guhl, I. Haase, U. Lippert, and T. Zuberbier. 1997. C3a and C5a stimulate chemotaxis of human mast cells. *Blood* 89: 2863–2870.
55. Hofstra, C. L., P. J. Desai, R. L. Thurmond, and W. P. Fung-Leung. 2003. Histamine H4 receptor mediates chemotaxis and calcium mobilization of mast cells. *J. Pharmacol. Exp. Ther.* 305: 1212–1221.

Downloaded from www.jimmunol.org on December 22, 2010

Changes in red

Legends to supplemental material

FIGURE S1. Correlation between formation of microtubule protrusions and degranulation in activated mast cells. Control or activated BMMCL cells were either fixed and stained for β-tubulin or used for determination of β-glucuronidase release. (A) IgE-sensitized (1 μg/ml) cells activated with different concentrations of Ag for 5 min. (B) Cells activated with different concentration of thapsigargin for 20 min. (C) IgE-sensitized cells activated with Ag (100 ng/ml) for various time intervals. (D) Cells activated with thapsigargin (2 μM) for various time. Three independent experiments were performed, each involving 500 cells and examined for the presence of microtubule protrusions. Values indicate means ± SD (n=3). Data for β-glucuronidase release represent means ± SD (n=3).

FIGURE S2. Activation of mast cells with Ag increases the number of growing microtubules in cell periphery as determined by TIRFM time-lapse imaging. (A) Time-lapse imaging of resting (a-b) and FcεRI aggregation-activated (c-d) BMMCL cells expressing EB1-GFP. Still images of EB1 (a, c) and tracks of EB1 comets over 20 sec created by maximum intensity projection of the 20 consecutive frames (b, d). Scale bar, 5 μm. (B) Histogram of microtubule growth rates in cell periphery of resting (-Ag) and Ag-activated (+Ag) cells. Total 10 different cells were tracked in 3 independent experiments. Values indicate mean ± SE, n=10 (*, $p<0.05$;**, $p<0.01$).

FIGURE S3. Degranulation and Ca^{2+} responses in cells with reduced STIM1 levels. (A-B) Changes in the degree of degranulation quantified as β-glucuronidase release. IgE-sensitized

(1 μg/ml) cells infected with empty pLKO.1 vector (Control) or cells with reduced STIM1 after infection with shRNA2 (KD2) were activated with different concentrations of DNP-albumin for 30 min (A) or thapsigargin for 20 min (B) and the release of β-glucuronidase was determined. Data in (A) and (B) represent means ± SD (n=3, both for controls and KD2). (C-D) Changes in $^{45}Ca^{2+}$ uptake. IgE-sensitized (1 μg/ml) control cells (empty pLKO.1vector) or STIM1 KD2 cells were activated for various time intervals with 100 ng/ml DNP-albumin (C) or 2 μM thapsigargin (D) in the presence of extracellular $^{45}Ca^{2+}$ (1 mM). Data in (C) and (D) represent means ± SD (n=6, both for controls and KD2). (E-F) Changes in intracellular Ca^{2+} mobilization. IgE-sensitized (1 μg/ml) control cells (empty pLKO.1vector) or STIM1 KD2 cells loaded with Fluo 3-AM were activated (arrows) by 100 ng/ml DNP-albumin (E) or 2 μM thapsigargin (F). Data in (E) and (F) represent means ± SD (n=3, both for controls and KD2). (***, $p<0.001$; in E and F the line under asterisks indicate time interval of significant differences).

Movie S1. Time-lapse imaging of EB1-GFP in quiescent cells. BMMCL cells were imaged, with 0.5 s exposure time and 1 s interval between frames, for 3 min in TIRFM.

Movie S2. Time-lapse imaging of EB1-GFP in thapsigargin activated cells. BMMCL cells were imaged, with 0.5s exposure time and 1 s interval between frames, for 3 min in TIRFM. Imaging started 13 min after addition of thapsigargin at final concentration 2 μM.

Movie S3. Time-lapse imaging of YFP-hSTIM1 in quiescent cells. BMMCL cells were imaged, with 0.5s exposure time and 1 s interval between frames, for 3 min in TIRFM.

Movie S4. Time-lapse imaging of YFP-hSTIM1 in the course of thapsigargin activation of cells. BMMCL cells were imaged, with 0.5s exposure time and 1 s interval between frames, for 3 min in TIRFM. Thapsigargin was added 30s after starting the movie.

Movie S5. Time-lapse imaging of YFP-hSTIM1 and EB3-mRFP1 in the course of nocodazole treatment of cells, folowed by thapsigargin activation. BMMCL cells were imaged, with exposure time ranging from 0.5-0.8s and 2 s interval between frames, for 3 min in TIRFM. Nocodazole and thapsigargin were added to the final concentration of 10 μM and 2 μM, respectively. Elapsed time in minutes and seconds is depicted in the upper right.

Fig. S1

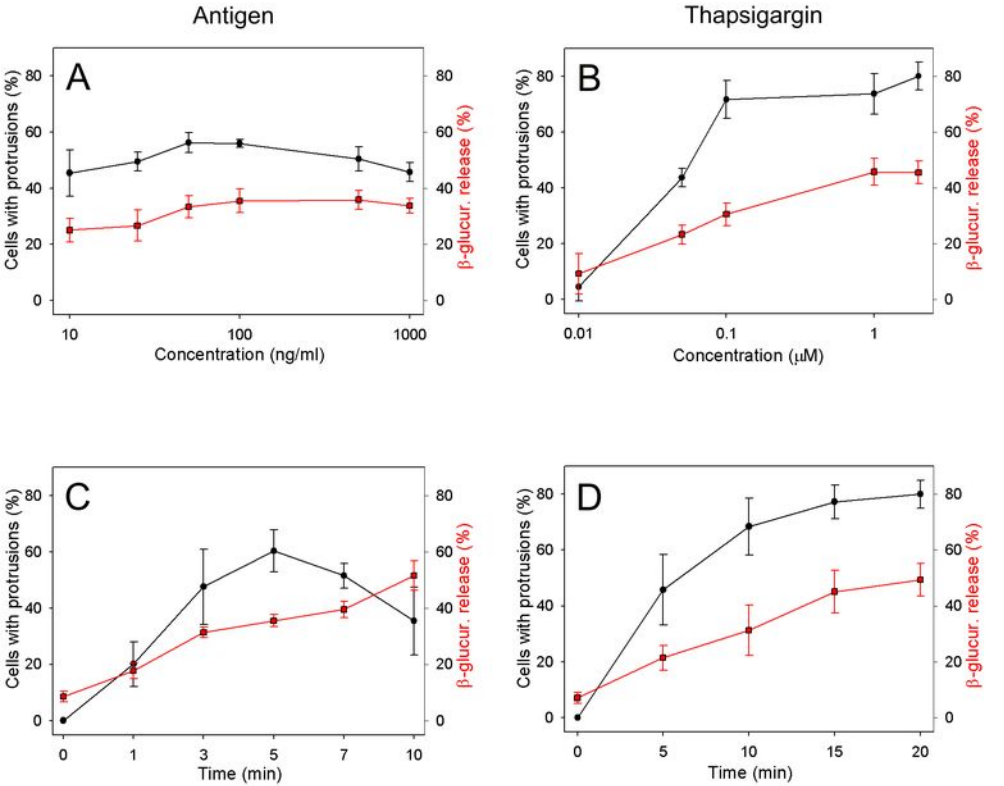
Antigen
Thapsigargin
A
B
C
D
Cells with protrusions (%)
β-glucur. release (%)
Concentration (ng/ml)
Concentration (μM)
Time (min)
0
20
40
60
80
10
100
1000
0.01
0.1
1
0
1
3
5
7
10
0
5
10
15
20

Fig. S2

A

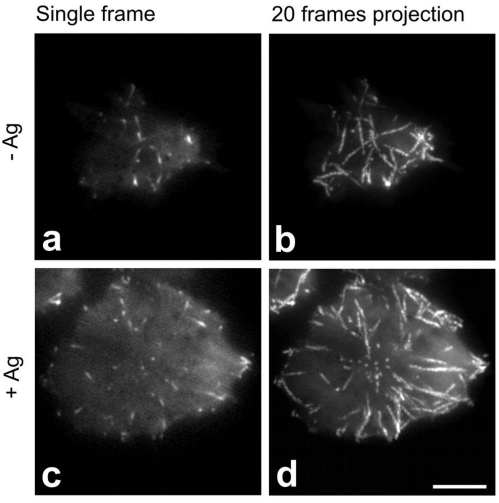
Single frame
20 frames projection
- Ag
+ Ag
a
b
c
d

B

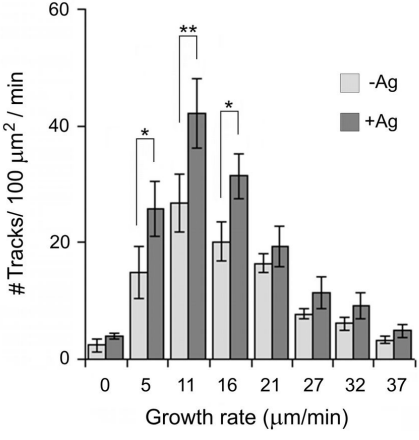
60
40
20
0
Tracks/ 100 μm² / min
*
**
*
-Ag
+Ag
0
5
11
16
21
27
32
37
Growth rate (μm/min)

Fig. S3

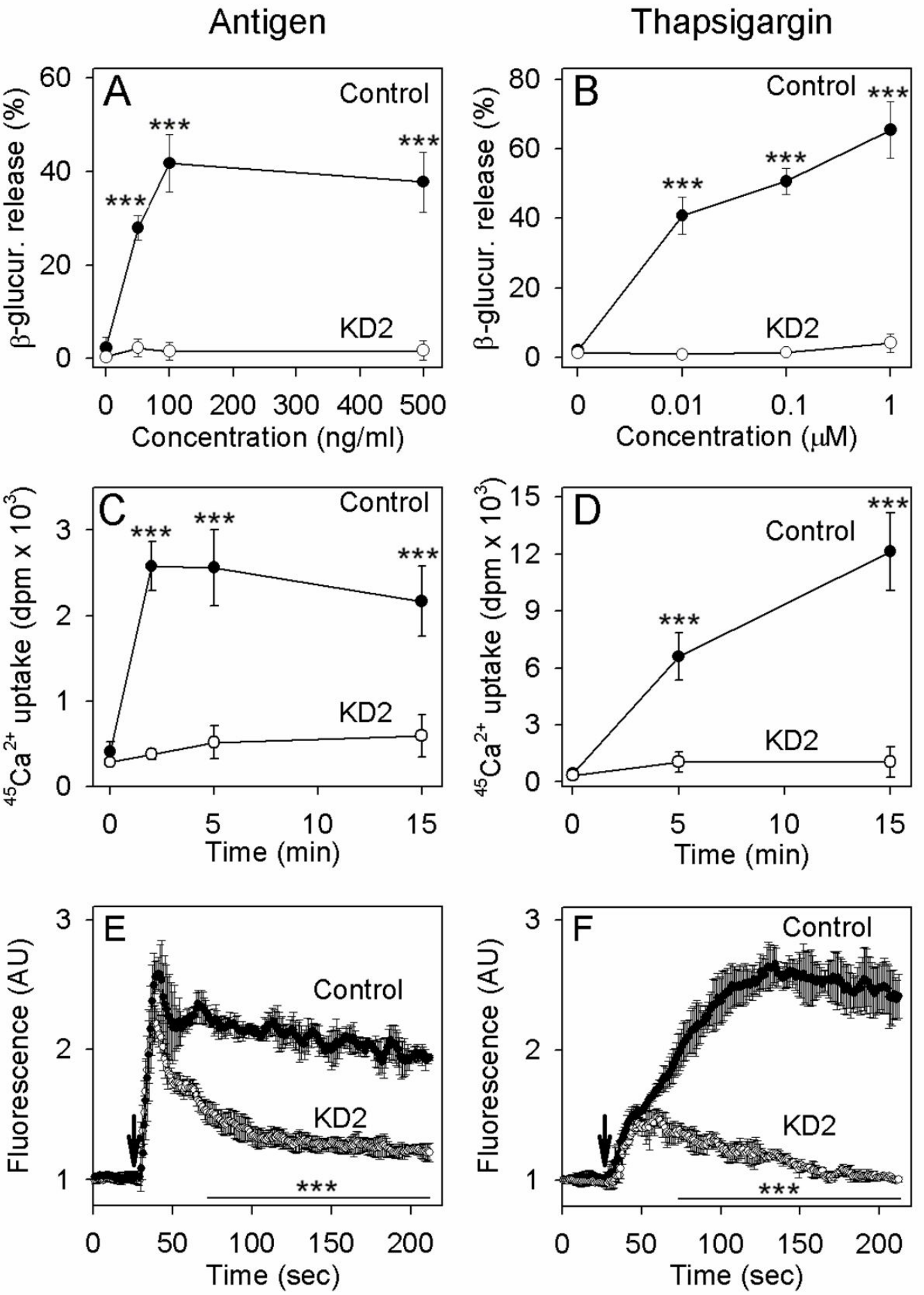
Antigen
Thapsigargin
A
Control
KD2
β-glucur. release (%)
Concentration (ng/ml)
B
Concentration (μM)
C
$^{45}Ca^{2+}$ uptake (dpm x 10^3)
Time (min)
D
E
Fluorescence (AU)
Time (sec)
F
***